Equation of state of pyrite to 80 GPa and 2400 K

Thompson, E.C.[1*], Chidester, B.A.[1], Fischer, R.A.[1,2], Myers, G.I. [1], Heinz, D.L.[1], Prakapenka, V.B.[3], Campbell, A.J.[1]

[1]Department of the Geophysical Sciences, University of Chicago, [2]Now at the National Museum of Natural History, Smithsonian Institution and the Department of Earth and Planetary Sciences, University of California Santa Cruz, [3]Center for Advanced Radiation Sources, University of Chicago

*Corresponding author. Tel: +1 504 460 7658

Email address: ecthompson@uchicago.edu (E. C. Thompson)

Submitted to *Am. Mineral.* August 10, 2015

Accepted by *Am. Mineral.* November 30, 2015

Abstract

The high cosmic abundance of sulfur is not reflected in the terrestrial crust, implying it is either sequestered in the Earth's interior or was volatilized during accretion. As it has widely been suggested that sulfur could be one of the contributing light elements leading to the density deficit of Earth's core, a robust thermal equation of state of iron sulfide is useful for understanding the evolution and properties of Earth's interior. We performed X-ray diffraction measurements on FeS_2 achieving pressures from 15 to 80 GPa and temperatures up to 2400 K using laser-heated diamond anvil cells. No phase transitions were observed in the pyrite structure over the pressure and temperature ranges investigated. Combining our new *P-V-T* data with previously published room temperature compression and thermochemical data, we fit a Debye temperature of 624(14) K and determined a Mie-Grüneisen equation of state for pyrite having bulk modulus K_T = 141.2(18) GPa, pressure derivative K_T' = 5.56(24), Grüneisen parameter γ_0 = 1.41, anharmonic coefficient $A_2 = 2.53(27)\times10^{-3}$ $JK^{-2}mol^{-1}$, and q = 2.06(27). These findings are compared to previously published equation of state parameters for pyrite from static compression, shock compression, and ab initio studies. This revised equation of state for pyrite is consistent with an outer core density deficit satisfied by 11.4(10) wt% sulfur, yet matching the bulk sound speed of PREM requires an outer core composition of 4.8(19) wt% S. This discrepancy suggests that sulfur alone cannot satisfy both seismological constraints simultaneously and cannot be the only light element within Earth's core, and so the sulfur content needed to satisfy density constraints using our FeS_2 equation of state should be considered an upper bound for sulfur in the Earth's core.

Keywords: high pressure, diamond anvil cell, equation of state, X-ray diffraction

Introduction

The Earth's outer liquid core is a layer approximately 2,300 kilometers thick, and contains 30% of the Earth's mass. Despite comprising such a large percentage of the Earth's bulk material, there remain uncertainties surrounding the composition of this region of the interior. It is accepted that the Earth's core is predominantly iron-nickel alloy, but with one or more lighter elements needed to compensate for the fact that the outer core is ~10% less dense (Birch 1952) and with a bulk modulus ~12% lower (Jeanloz 1979) than pure iron under appropriate pressure-temperature (*P*-*T*) conditions. Several potential light elements have been proposed to account for these differences, notably silicon, carbon, oxygen, hydrogen, and sulfur because of their high cosmochemical abundances and affinity for iron metal (e.g., Poirier 1994; McDonough 2003). While it is likely that a combination of these light elements is needed to account for the Earth's core density deficit, it is important to constrain the maximum of each element's contribution by comparing equations of state against the density and compressibility of the outer core based on seismological models (e.g., Preliminary Reference Earth Model) (Dziewonski and Anderson 1981).

Understanding the distribution of sulfur within Earth is a primary concern because of sulfur's direct impact on the physical and chemical properties of solids, magmas, and alloy melts. Volatiles including sulfur play an important role in defining the geochemical environment during Earth's accretion (Walter et al. 2000), and sulfur has been found to greatly influence the metal–silicate partitioning behavior of some elements (Wood et al. 2014). Furthermore, the addition of even small weight percent quantities of sulfur to Fe–Si, Fe–O, or Fe–C melts can produce two immiscible phases at low pressures (Raghavan 1998), and can reduce the surface

tension, compressibility, and melting temperature of these melts (Sanloup et al. 2000; Andrault et al. 2009). These influences are important during the differentiation of young terrestrial planets.

Sulfur's volatile yet moderately siderophile nature makes it likely that during Earth's differentiation some unknown fraction of sulfur was volatilized, yet a significant fraction may have been incorporated into the Earth's core. In fact, Wood et al. (2014) found that a complete absence of sulfur in the core would be irreconcilable with the observed Mo and W abundances in the mantle, leading to an overabundance of W relative to Mo in the Earth's core due to sulfur's influence on the relative metal–silicate partitioning of both elements. Recent findings of mid-ocean ridge basalts with $^{34}S/^{32}S$ ratios depleted relative to chondritic values are consistent with isotopic sulfur fractionation between the silicate mantle and the iron core during early planetary differentiation (Labidi et al. 2013, 2014), and indicate that sulfur may contribute significantly to the light element budget of the core, consistent with high pressure partitioning experiments on Fe–S–silicate systems (Li and Agee 2001; Li et al. 2001) which show that sulfur's affinity for iron increases with pressure .

Pyrite, the cubic (*Pa3*) form of FeS_2, is the most commonly found sulfide mineral in Earth's crust, and exists in a range of geological settings including sedimentary beds, as a replacement mineral in fossils, and in metamorphic rocks. The geological abundance of pyrite may not be limited to the sampled crust and upper mantle, as shock experiments by Ahrens and Jeanloz (1987) suggest pyrite is stable to pressures of 320 GPa without a pressure-induced phase change. The geological abundance, wide stability range, and the potential for sulfur to be a dominant light element in Earth's outer core all render pyrite FeS_2 a vital material for study at high *P*-*T* conditions.

Because of its geological importance, previous efforts have been made to establish a high-temperature equation of state (EoS) for pyrite FeS_2 (Chattopadhyay and von Schnering 1984; Merkel et al. 2002; Whitaker et al. 2010). Yet, limited pressure ranges and non-hydrostatic stress conditions weaken the extrapolation of these static-compression studies to core–mantle boundary (CMB) conditions. Although dynamic compression experiments (Ahrens 1987; Ahrens and Jeanloz 1987; Anderson and Ahrens 1996) and first-principles calculations (Muscat et al. 2002; LePage and Rodgers 2005; Blanchard et al. 2005; Umemoto et al. 2014) have also bolstered our understanding of the material properties of pyrite under elevated *P*-*T* conditions, there remains a lack of consensus between studies that necessitates revisiting the development of a thermal equation of state for cubic FeS_2 that can be extrapolated to CMB conditions to benchmark the maximum possible sulfur content of the outer core.

Experimental Methods

The FeS_2 used in this study was obtained from Alfa Aesar (Stock 12342, 99.9%). It was ball milled for 45 minutes at 20 Hz, then pressed between diamonds to form platelets 5–10 μm thick and approximately 50 μm in diameter, before being loaded into symmetric diamond anvil cells (DACs). Unlike several other sulfides, pyrite FeS_2 does not vary significantly from its stoichiometric ideal (Ellmer and Höpfner 1997). The zero-pressure, room-temperature volume of our ball-milled sample material was obtained using X-ray diffraction (XRD) at the University of Chicago using a Bruker B8 Powder X-ray diffractometer, and was found to be 23.93(1) cm^3/mol, consistent with previously published volumes for stoichiometric FeS_2 (Whitaker et al. 2010).

Pyrite samples for laser heating were loaded between two platelets of KBr each ~10 μm thick, which served as an insulator, pressure medium, and pressure standard. Powdered KBr was baked prior to being compressed into platelets, and prepared sample assemblies were baked for

an additional hour at 100° C prior to closing the DACs, to mitigate the effect of water absorption. Samples for room temperature compression were prepared by mixing powdered FeS_2 with gold with a grain size of 0.5–0.8 μm obtained from Alfa Aesar (Stock 44636, 99.96+%) as a pressure standard. Neon, used as a hydrostatic pressure medium during room temperature compression, was loaded as a pressurized gas at the Advanced Photon Source using the COMPRES/GSECARS gas-loading system (Rivers et al. 2008).

Angle-dispersive X-ray diffraction experiments were performed at beamlines 13-ID-D (GSECARS) and 16-ID-B (HP-CAT) at the Advanced Photon Source, Argonne National Laboratory. Laser-heating experiments and room temperature compression experiments were conducted at 16-ID-B using a monochromatic incident X-ray beam (λ = 0.406626 Å) of 6 μm by 7.5 μm at full-width at half-maximum of the focused spot. Laser-heating experiments were also performed at 13-ID-D with a monochromatic incident X-ray beam (λ = 0.3344 Å) of 3 μm by 4 μm at full-width at half-maximum of the focused spot. Sample-to-detector distances and tilt were calibrated using 1-bar diffraction of CeO_2 or LaB_6. The laser was aligned with the X-ray beam using the X-ray induced fluorescence of the KBr pressure medium, and laser-heating temperatures were determined via spectroradiometry using the greybody approximation (Prakapenka et al. 2008; Meng et al. 2006). Samples were laser heated simultaneously on both sides, laser power was adjusted to balance upstream and downstream temperatures, and axial temperature gradients due to sample thickness were taken into account (3% correction) using the procedure previously described by Campbell et al. (2007, 2009).

Diffraction patterns were integrated to produce 2θ plots using FIT2D (Hammersley et al. 1996) and DIOPTAS (Prescher and Prakapenka 2015), and the resultant integrated patterns were fit to determine lattice parameters as a function of pressure and temperature using PeakFit (Systat

Software). Individual peaks were fit to single Gaussian curves, and unresolved overlapping peaks were not used in the calculation of lattice parameters. Unit-cell volumes of pyrite (FeS_2) were calculated from the lattice parameters determined from a least-squares fitting using at minimum the following *hkl* peaks: 111, 200, 211, 220, 311, and 321 (Figure 1). Pressures in laser-heated samples were determined using the Dewaele et al. (2012) equation of state for B2-KBr with temperatures adjusted for axial temperature gradients within the insulator as described by Campbell et al. (2009). Pressures in room temperature compression samples were determined using the Dorogokupets and Oganov (2007) equation of state for gold, which is inter-calibrated with the Dewaele et al. (2012) B2-KBr equation of state, allowing for direct comparison of the pressures between these samples.

Results and Discussion

Equation of State

In agreement with previous dynamic and static compression experiments (Ahrens and Jeanloz 1987; Merkel et al. 2002), no phase transitions were observed in the cubic (*Pa*3) pyrite structure over the pressure and temperature ranges investigated in this study. There were no substantial changes in relative intensity of diffraction peaks observed and no significant peak broadening that would indicate evolving deviatoric stresses during room-temperature compression. Pressure-volume-temperature (*P*-*V*-*T*) data from these synchrotron experiments are listed in Supplemental Table S1. The unit cell volumes calculated from the measured lattice parameters of our study exhibit a smoothly decreasing trend with increasing pressure (Figure 2).

We can describe the room temperature *P*-*V* data acquired from our synchrotron XRD experiments using a Vinet equation of state (Vinet et al. 1987) of the form:

$$P_{300}(V) = 3K_T\left(\frac{1-\eta}{\eta^2}\right)e^{\frac{3}{2}(K_T'-1)(1-\eta)}$$

in which K_T is the isothermal bulk modulus at 1 bar, K_T' is the derivative of the isothermal bulk modulus with respect to pressure at 1 bar, and $\eta = (V/V_0)^{1/3}$ with initial volume V_0. Our room temperature data was supplemented by Ne-loaded room temperature data from Merkel et al (2002), which is plotted alongside our data in Figure 2. The quality of fit to the room temperature data from both this study and Merkel et al. (2002) is illustrated in an *f-F* plot in Figure S1. Trade-offs between the fitted values for K_T' and K_T (Table 1) are given in the form of a covariance ellipse in Figure 3. This Vinet equation defines a 300 K isothermal pressure P_{300} to which harmonic (Debye-like) and anharmonic (A_2) thermal terms were added to give a *P-V-T* equation state of the form:

$$P(V,T) = P_{300}(V) + (\gamma/V)[E_D(T) - E_D(300) + \tfrac{1}{2}A_2(T^2 - 300^2)]$$

which describes thermal pressure in terms of a Debye-like vibrational energy function $E_D(T)$ plus an anharmonic term with coefficient A_2, where T is in Kelvin. Here the Grüneisen parameter is $\gamma = \gamma_0(V/V_0)^q$ and the Debye temperature (θ_D) varies as $\mathrm{dln}\theta_D/\mathrm{dln}V = -\gamma$.

Reference values (at 1 bar, 300 K) for the Grüneisen parameter (γ_0) and isentropic bulk modulus (K_S) were obtained by simultaneously satisfying the relations $\gamma_0 = (\alpha K_S V_0)/C_P$ and $K_S = K_T(1+\alpha\gamma_0 T)$, using literature values of thermal expansion (α) and heat capacity at constant pressure (C_P) (Table 2) with our measured K_T and V_0. The anharmonic coefficient A_2, which also includes electronic effects, can be related to the difference between the observed heat capacity and the harmonic (Debye) heat capacity:

$$A_2 = \left\{ \left(\frac{C_P}{1 + \alpha\gamma_0 T} \right) - 9R \left[3 \left(\frac{T}{\theta_D} \right)^3 \int_0^{\frac{\theta_D}{T}} \frac{x^4 e^x}{(e^x - 1)^2} \, dx \right] \right\} \div T$$

Here the A_2 coefficient and the one-bar Debye temperature (θ_D) were fit using published C_P data (Robie et al. 1978), a polynomial expression for thermal expansion as a function of temperature

(Fei 1995), and the γ_0 obtained above. These values were then held fixed when fitting our high temperature, high pressure X-ray diffraction data, allowing us to tightly constrain the higher order term q in the thermal equation of state. We tested for a volume dependence of the A_2 term and found it was unresolvable. Self-consistent values of K_T, K_T', γ_0, A_2, and q were determined using both the Vinet and Birch-Murnaghan (Birch 1952) formalisms (Table 1).

Our equation of state parameters are compared to previous experimentally derived fits and ab initio calculations for pyrite FeS_2 (Table 1). In general, we find good agreement with experimental studies (Merkel et al. 2002; Whitaker et al. 2008; Drickamer et al. 1967) (Figure 3), although the higher-pressure range of our data allowed a more precise determination of K_T'. In contrast, both ab initio studies (Blanchard et al. 2005; LePage and Rogers 2005) have systematically higher K_T values and correspondingly lower K_T' values than experimental results, possibly due to their computational methods, which attempt to describe the covalently bonded pyrite using interatomic potentials better suited to the description of ionic compounds. Furthermore, our equation of state (using Vinet parameters) was used to calculate a Hugoniot compression curve (e.g., Ahrens 1987), which is in reasonable agreement with previously published shock data from Ahrens and Jeanloz (1987), although scatter in the shockwave data limits the quality of the fit (Supplemental Figure S2).

Sulfur in Earth's core

The Earth's iron-alloy core exhibits different material properties than are expected of pure iron under the same *P-T* conditions. It is expected that the inclusion of one or more light elements in the core is responsible for the differences in density and sound wave velocities between pure iron and seismically determined values (e.g., Birch 1952). Our experimentally derived equation of state has been used to compare the density and bulk sound speed of FeS_2 to

those of hcp-iron (Dewaele et al. 2006) and PREM (Dziewonski and Anderson 1981) to constrain the maximum amount of S in the Earth's core (Figure 4). To enable this calculation the following constraints were applied: (1) a pressure of 135.8 GPa, density of 9.9 g/cm^3, and a bulk sound speed of 8.07 km/s at the CMB (Dziewonski and Anderson 1981), (2) a CMB temperature of 4000 ± 500 K (Anderson 2003), (3) an adiabatic temperature profile throughout the outer core (Birch 1952), (4) an increase of 1.5 ± 0.5% in the volume of both iron and iron alloys upon melting at core pressures (Anderson 2003), and (5) the mean atomic weight was adjusted to account for the inclusion of 5:95 Ni:Fe. Bulk sound speeds, equivalent to V_P in the outer core, were calculated numerically from the slope of an adiabatic pressure–density profile. Constraining the quantity of a single light element within the Earth's outer core using the equation of state of a solid with the addition of a term to account for volume change due to melting has been employed by numerous previous studies (e.g., Seagle et al. 2006). Consistent with previous findings (Lin et al. 2003) small variations in the added wt% of Ni did not significantly alter the bulk sound speed of iron.

For this analysis only sulfur is considered as a contributing light element of the outer core, despite the likelihood that the observed core properties are the result of several light elements (e.g., Si, O, C) in combination (e.g., Poirier et al. 1994). By comparing modeled core compositions using the Vinet equation of state parameters presented here against PREM, maximum sulfur contents of the outer core were determined. Modeled compositions using the Birch-Murnaghan equation of state formalism yielded indistinguishable results. The best-fit compositional model to the core density deficit of PREM suggests that if sulfur were the only light element in the core, then the outer core's sulfur content would be 11.4(10) wt%, with deviations due to variations in CMB temperature and the volume change due to melting. This

value is very similar to the 11(2) wt% S inside the outer core proposed by Ahrens and Jeanloz (1987) based on matching the density of PREM using dynamic compression data. Additionally, the sulfur content presented here is in good agreement with estimates using other iron sulfide compositions including pyrrhotite (9–12 wt%, Ahrens 1979; 10(4) wt%, Brown et al. 1984) and Fe_3S (12.4(20) wt%, Seagle et al. 2006). However, comparing modeled core compositions to the bulk sound speed of PREM instead of its density, the best-fit model suggests an outer core composition of only 4.8(19) wt% S. This result is still higher than the 2.4 wt% maximum proposed by Badro et al. (2014) based on molecular dynamics simulations of sound velocities and densities of multi-light element systems. Calculating the sulfur content of the inner core using a similar methodology and an inner core boundary temperature of 5000 ± 500 K requires 4.1(12) wt% S based on matching PREM density, or 4.7(29) wt% S matching PREM bulk sound speed. According to our findings, the density and bulk sound speed in PREM may not be matched simultaneously with a single iron-sulfur alloy composition. This result strengthens the argument for additional light elements in Earth's core, and as such the 11.4 wt% S content derived from our FeS_2 equation of state should be considered a conservative upper bound for sulfur in the outer core's light element budget.

Implications

In contrast to many geophysically important compounds, pyrite FeS_2 exhibits no structural phase transitions at high *P-T* conditions that would complicate the measurement of its equation of state. Consequently, in this study we were able to fix many important equation of state parameters to their values at ambient conditions, and apply our new experimental *P-V-T* data to obtain the higher order terms in the FeS_2 equation of state—namely K_T', q, and A_2. Additionally, we refit the Debye temperature using previously published thermodynamic data in

conjunction with our new equation of state parameters, allowing for a greater level of self-consistency. Hence, the equation of state presented here has a more complex and realistic form than most experimentally derived thermal equations of state for deep Earth materials, and can therefore be extrapolated to higher *P*-*T* conditions with greater accuracy. In particular, we find a *q* value that is significantly greater than the value of 1.0 that is commonly assumed, and we find a significant anharmonic coefficient ($A_2 = 2.53(27)\times10^{-3}$ $JK^{-2}mol^{-1}$) for pyrite. This anharmonic term accounts for ~6-8% of the thermal pressure at CMB conditions and even more at conditions deeper into the core.

Regarding the application of this equation of state to the composition of Earth's core, our results are compatible with earlier indications that sulfur alone cannot account for the entire light element budget of the outer core (Ringwood 1984; Dreibus and Palme 1996). This study is a contribution to the broad effort to constrain the composition of Earth's core by combining mineral physics data with seismological observations of our planet's deep interior. Comparison of the FeS_2 and Fe equations of state to PREM allows one to calculate a maximum contribution of sulfur to the light element budget of the outer core. Yet while high-pressure experiments indicate sulfur strongly partitions into the iron cores of terrestrial planets (e.g., Li and Agee 2001), further investigation is needed to determine the likelihood that sulfur is a major contributor Earth's core density deficit. In particular it is important to understand whether sulfur was lost from Earth to the same degree as some volatile lithophile elements, as is sometimes assumed (Dreibus and Palme 1996; McDonough 2003). Metal–silicate partitioning studies at high *P*-*T* conditions will also be helpful to understand how sulfur was distributed between the proto-core and proto-mantle during differentiation of the Earth.

Acknowledgements

We thank the editors and the two reviewers for their helpful comments on the manuscript. This research is supported by National Science Foundation Graduate Research Fellowships to E.C.T. and B.A.C., an American Association of University Women Educational Foundation Dissertation Fellowship to R.A.F., and National Science Foundation Grant # EAR-1427123 to A.J.C. This work was completed at HPCAT (Sector 16) and GeoSoilEnviroCARS (Sector 13), Advanced Photon Source (APS), Argonne National Laboratory. HPCAT operations are supported by DOE-NNSA under Award No. DE-NA0001974 and DOE-BES under Award No. DE-FG02-99ER45775, with partial instrumentation funding by NSF. GeoSoilEnviroCARS is supported by the National Science Foundation - Earth Sciences (EAR-1128799) and Department of Energy- GeoSciences (DE-FG02-94ER14466). This work was made possible by the generous assistance of the APS beamline scientists at both Sector 13 and Sector 16. The Advanced Photon Source is a U.S. Department of Energy (DOE) Office of Science User Facility operated for the DOE Office of Science by Argonne National Laboratory under Contract No. DE-AC02-06CH11357. Use of the COMPRES-GSECARS gas loading system was supported by COMPRES under NSF Cooperative Agreement EAR 11-57758 and by GSECARS through NSF grant EAR-1128799 and DOE grant DE-FG02-94ER14466. This research used resources of the Advanced Photon Source, a U.S. Department of Energy (DOE) Office of Science User Facility operated for the DOE Office of Science by Argonne National Laboratory under Contract No. DE-AC02-06CH11357.

References Cited

Ahrens, T.J. (1987) Shock wave techniques for geophysics and planetary physics. In C.G. Sammis and T.L. Henyey, Eds., Geophysics, Laboratory Experiments, p. 185. Academic, San Diego, C.A.

Ahrens, T.J., and Jeanloz, R. (1987) Pyrite: Shock compression, isentropic release, and composition of the Earth's core. Journal of Geophysical Research, 92, 363–375.

Anderson, O.L. (2003), The three-dimensional phase diagram of iron. In V. Dehant, K.C. Creager, S.-I. Karato, and S. Zatman, Eds., Earth's Core: Dynamics, Structure, Rotation, p. 83–103. American Geophysical Union, Washington, D.C.

Anderson, W., and Ahrens, J. (1996) Shock temperatures and melting in iron sulfides at core pressures. Journal of Geophysical Research, 101, 5627–5642.

Andrault, D., Bolfan-Casanova, N., Ohtaka, O., Fukui, H., Arima, H., Fialin, M., and Funakoshi, K. (2009) Melting diagrams of Fe-rich alloys determined from synchrotron in situ measurements in the 15-23 GPa pressure range. Physics of the Earth and Planetary Interiors, 174, 181–191.

Badro, J., Côté, A.S., and Brodholt, J.P. (2014) A seismologically consistent compositional model of Earth's core. Proceedings of the National Academy of Sciences of the United States of America, 111, 7542–7545.

Birch, F. (1952) Elasticity and constitution of the Earth's interior. Journal of Geophysical Research, 37, 227–286.

Blanchard, M., Alfredsson, M., Brodholt, J., Price, G.D., Wright, K., and Catlow, C.R.A. (2005) Electronic Structure Study of the High-Pressure Vibrational Spectrum of FeS_2 Pyrite. Journal of Physical Chemistry B, 109, 22067–22073.

Brown, J.M., Ahrens, T.J., and Shampine, D.L. (1984) Hugoniot data for pyrrhotite and the Earth's core. Journal of Geophysical Research, 89, 6041-6048.

Campbell, A.J., Seagle, C.T., Heinz, D.L., Shen, G., and Prakapenka, V.B. (2007) Partial melting in the iron–sulfur system at high pressure: A synchrotron X-ray diffraction study. Physics of the Earth and Planetary Interiors, 162, 119–128.

Campbell, A.J., Danielson, L., Righter, K. Seagle, C.T., Wang, Y., and Prakapenka, V.B. (2009) High pressure effects on the iron–iron oxide and nickel–nickel oxide oxygen fugacity buffers. Earth and Planetary Science Letters, 286, 556–564.

Chattopadhyay, T., and von Schnering, H.G. (1985) High pressure X-ray diffraction study on p-FeS_2, m-FeS_2 and MnS_2 TO 340 kbar: a possible high spin-low spin transition in MnS_2. Journal of Physics and Chemistry of Solids, 46, 113–116.

Dewaele, A., Loubeyre, P., Occelli, F., Mezouar, M., Dorogokupets, P.I., and Torrent, M. (2006) Quasihydrostatic equation of state of iron above 2 Mbar. Physical Review Letters, 97, 215504.

Dewaele, A., Belonoshko, A. B., Garbarino, G., Occelli, F., Bouvier, P., Hanfland, M., and Mezouar, M. (2012) High-pressure–high-temperature equation of state of KCl and KBr. Physical Review B, 85, 214105.

Dorogokupets, P.I., and Oganov, A.R. (2007) Ruby, metals, and MgO as alternative pressure scales: A semiempirical description of shock- wave, ultrasonic, x-ray, and thermochemical data at high temperatures and pressures. Physical Review B, 75, 1–16.

Dreibus, G., and Palme, H. (1996) Cosmochemical constraints content in the Earth's core. Geochimica et Cosmochimica Acta, 60, 1125–1130.

Drickamer, H.G., Lynch, R.W., Clendenen, R.L., and Perez-Albueene, E.A. (1967) X-Ray Diffraction Studies of the Lattice Parameters of Solids under Very High Pressure. Solid State Physics, 19, 135–228.

Dziewonski, A.M., and Anderson, D.L. (1981) Preliminary reference Earth model. Physics of the Earth and Planetary Interiors, 25, 297–356.

Ellmer, K., and Höpfner, C. (1997) On the stoichiometry of the semiconductor pyrite (FeS_2). Philosophical Magazine A, 75, 1129-1151.

Fei, Y. (1995) Thermal expansion. In T.J. Ahrens, Ed., Mineral Physics & Crystallography: A Handbook of Physical Constants, 2, p. 29–44. American Geophysical Union, Washington, D.C.

Hammersley, A.O., Svensson, S.O., Hanfland, M., Fitch, A.N., and Hausermann, D. (1996) Two-dimensional detector software: from real detector to idealized image or two-theta scan. High Pressure Research, 17, 235–248.

Jeanloz, R. (1979) Properties of iron at high pressures and the state of the core. Journal of Geophysical Research, 84, 6059–6069.

Labidi, J., Cartigny, P., and Moreira, M. (2013) Non-chondritic sulphur isotope composition of the terrestrial mantle. Nature, 501, 208–11.

Labidi, J., Cartigny, P., Hamelin, C., Moreira, M., and Dosso, L. (2014) Sulfur isotope budget (^{32}S, ^{33}S, ^{34}S and ^{36}S) in Pacific–Antarctic ridge basalts: A record of mantle source heterogeneity and hydrothermal sulfide assimilation. Geochimica et Cosmochimica Acta, 133, 47–67.

Le Page, Y., and Rodgers, J.R. (2005) Ab initio elasticity of FeS_2 pyrite from 0 to 135 GPa. Physics and Chemistry of Minerals, 32, 564–567.

Li, J., and Agee, C.B. (2001) Element partitioning constraints on the light element composition of the Earth's core, Geophysical Research Letters, 28, 81–84.

Li, J., Fei, Y., Mao, H.K., Hirose, K., and Shieh, S.R. (2001) Sulfur in the Earth's inner core. Earth and Planetary Science Letters, 193, 509–514.

Lin, J.-F., Struzhkin, V.V., Sturhahn, W., Huang, E., Zhao, J., Hu, M.Y., Alp, E.E., Mao, H., Boctor, N., and Hemley, R.J. (2003) Sound velocities of iron–nickel and iron–silicon alloys at high pressures. Geophysical Research Letters, 30, 2112.

McDonough, W.F. (2003) Compositional model for the Earth's core. In: R.W. Carlson, Ed., Treatise of Geochemistry, 2, p. 547–568. Elsevier-Pergamon, Oxford, U.K.

Meng, Y., Shen, G., and Mao, H.K. (2006) X-Ray Diffraction At High Pressures and High Temperatures. Journal of Physics: Condensed Matter, 18, S1097–S1103.

Merkel, S., Jephcoat, A.P., Shu, J., Mao, H.-K., Gillet, P., and Hemley, R.J. (2002) Equation of state, elasticity, and shear strength of pyrite under high pressure. Physics and Chemistry of Minerals, 29, 1–9.

Muscat, J., Hung, A., Russo, S., and Yarovsky, I. (2002) First-principles studies of the structural and electronic properties of pyrite FeS_2. Physical Review B, 65, 054107.

Poirier, J. (1994) Light elements in the Earth's outer core: A critical review. Physics of the Earth and Planetary Interiors, 85, 319–337.

Prakapenka, V.B., Kuba, A., Kuznetsov, A., Laskin, A., Shkurikhin, O., Dera, P., Rivers, M.L., and Sutton, S.R. (2008) Advanced flat top laser heating system for high pressure research at GSECARS: Application to the melting behavior of germanium. High Pressure Research, 28, 225–235.

Prescher, C. and Prakapenka, V.B. (2015) DIOPTAS: a program for reduction of two-dimensional X-ray diffraction and data exploration. High Pressure Research, DOI: 10.1080/08957959.2015.1059835.

Raghavan, V. (1998) Fe-O-S (iron-oxygen-sulfur). Journal of Phase Equilibria, 19, 273–274.

Ringwood, A.E. (1984) The Earth's core: its composition, formation and bearing upon the origin of the Earth. Proceedings of the Royal Society of London, A395, 1-46.

Rivers, M., Prakapenka, V., Kubo, A., Pullins, C., Holl, C., and Jacobsen, S. (2008) The COMPRES/GSECARS gas-loading system for diamond anvil cells at the Advanced Photon Source. High Pressure Research, 28, 273–292.

Robie, R.A., Hemingway, B.S., and Fisher, J.R. (1978) Thermodynamic properties of minerals and related substances at 298.15K and 1 bar (10^5 pascals) pressure and at higher temperatures. United States Geological Survey Bulletin, 1452, 1–464.

Sanloup, C., Guyot, F., Gillet, P., Fiquet, G., Mezouar, M., and Martinez, I. (2000) Density measurements of liquid Fe-S alloys at high-pressure. Geophysical Research Letters, 27, 811–814.

Seagle, C.T., Campbell, A.J., Heinz, D.L., Shen, G., and Prakapenka, V.B. (2006) Thermal equation of state of Fe_3S and implications for sulfur in the Earth's core. Journal of Geophysical Research, 111, DOI: 10.1029/2005JB004091.

Umemoto, K., Hirose, K., Imada, S., Nakajima, Y., Komabayashi, T., Tsutsui, S., and Baron, A.Q.R. (2014) Liquid iron-sulfur alloys at outer core conditions by first-principles calculations. Geophysical Research Letters, 41, 6712–6717.

Vinet, P., Ferrante, J., Rose, J.H. and Smith, J.R. (1987) Compressibility of solids. Journal of Geophysical Research, 92, 9319–9325.

Walter, M.J., Newsom, H.E., Ertel, W., and Holzheid, A. (2000) Siderophile elements in the Earth and Moon: metal/silicate partitioning and implications for core formation. In: R.M. Canup and K. Righter, Eds., Origin of the Earth and Moon, p. 265–289. University of Arizona Press, Tucson.

Whitaker, M.L., Liu, W., Wang, L., and Li, B. (2010) Acoustic velocities and elastic properties of pyrite (FeS_2) to 9.6 GPa. Journal of Earth Science, 21, 792–800.

Wood, B.J., Kiseeva, E.S., and Mirolo, F.J. (2014) Accretion and core formation: The effects of sulfur on metal–silicate partition coefficients. Geochimica et Cosmochimica Acta, 145, 248–267.

Figure Captions

Figure 1. Representative background subtracted, integrated X-ray diffraction spectra collected on heating at 58 GPa and 2033 K.

Figure 2. Vinet equation of state of pyrite-FeS_2 up to 80 GPa. Circles are measured volumes from this study, triangles are data from Merkel et al. (2002), and color-coded dashed lines are isotherms calculated at the median temperature of the data within each indicated temperature range.

Figure 3. Comparison of K_T and K_T' values for this study to previously published results. The covariance ellipses of K_T–K_T' are based on the 2σ-uncertainties of our fit. Circles: DAC w/XRD. ×'s: ab initio calculations. Square: Ultrasonics w/XRD. Triangle: High-pressure apparatus w/XRD (no primary pressure standard used).

Figure 4. Influence of added FeS_2 on (**a**) core density deficit and (**b**) bulk sound speed. Solid lines indicate densities along an adiabatic temperature profile for a CMB temperature of 4000 K.. Red: FeS_2 calculated from the parameters listed in Table 1 with dashed lines denoting the uncertainty due to ±500 K temperature uncertainty at the CMB and the 95% confidence interval of the fit to experimental data. Blue: hcp-Fe calculated from the equation of state of Dewaele et al. (2006) with dashed lines denoting a ±500 K temperature uncertainty at the CMB. Green: mixture of FeS_2 and hcp-Fe with molar ratio fixed to fit PREM at CMB with dashed lines indicating weighted averages of iron and pyrite uncertainties; (**a**) shows the effect of 11.1(10) wt% S and (**b**) is best fit by 4.4(4) wt% S.

Supplemental Figure S1. Normalized stress as a function of Eulerian strain. Red circles: Room temperature data from this study. Grey circles: Room temperature data from Merkel et al. (2002). Black line calculated from the Birch Murnaghan equation of state parameters, illustrating quality of fit to the data.

Supplemental Figure S2. Comparison of projected Hugoniot against previous shock data. The lowest pressure datum was not fit by Ahrens and Jeanloz (1987) in obtaining EoS parameters as its peak pressure was below the Hugoniot elastic limit. Black line: 300 K isotherm. Red line: Hugoniot based on current study. Grey circles: Ahrens and Jeanloz (1987) data points. Errors reported by that study are within the size of the symbol.

Tables

Table 1. Equation of state parameters. Values in parentheses are uncertainties.

Ref.	Method	K_{T0} [GPa]	K_{T0}'	γ_0	q	A_2 [10^{-3} $JK^{-2}mol^{-1}$]
1a	LH-DAC w/XRD	139.7(15)	5.69(19)	1.39	2.04(28)	2.53(27)
1b	LH-DAC w/XRD	140.2(15)	5.52(19)	1.40	2.14(29)	2.51(45)
2	HPA w/XRD	148	5.5	-	-	
3	DAC w/XRD	215	5.5	-	-	
4	DAC w/XRD	133.5(52)	5.73(58)	-	-	
5	US w/XRD	137.5	6.0	-	-	
5	MA w/XRD	137.51(1)	6.01(1)	-	-	
6	ab initio calculation	150.0	4.56	-	-	
7	ab initio calculation	176.21	4.65	-	-	

1a. This study, fit to a Vinet equation of state; 1b. This study, fit to a Birch-Murnaghan equation of state; 2. Drickamer et al. (1967); 3. Chattopadhyah and von Schnering (1985); 4. Merkel et al. (2002); 5. Whitaker et al. (2010); 6. LePage and Rogers (2005); 7. Blanchard et al (2005). LH: laser-heated; DAC: diamond anvil cell; XRD: X-ray diffraction; HPA: high pressure apparatus, MA: multi-anvil; US: ultrasonics.

Table 2. Room temperature parameters used in EoS fitting. Uncertainties provided in parentheses when available.

Ref.	Parameter	Value
1, 2	α [K^{-1}]	25.7×10^{-6}
3	C_P [$Jmol^{-1}K^{-1}$]	62.17
4	θ_D [K]	624(14)
4	V_0 [cm^3/mol]	23.93(1)

1. Fei (1995); 2. Anderson and Ahrens (1996); 3. Robie et al. (1978); 4. This study.

Supplemental Table S1. Pyrite *P-V-T* data. Values in parentheses are uncertainties.

Sample-Pattern	Pressure (GPa)	Volume (cm^3/mol)	Temperature (K)
B9-333	16.40(24)	22.299(04)	1917(132)
B9-337	15.28(25)	22.456(10)	1763(124)
B9-343	15.66(24)	22.185(10)	1565(123)
B9-346	14.75(24)	22.399(11)	1422(120)
B9-349	15.48(26)	22.159(10)	1347(127)
B9-370	25.87(21)	21.488(65)	1966(119)
B9-374	24.45(21)	21.832(75)	2063(114)
B9-379	24.22(21)	21.759(12)	1915(115)
B9-425	45.07(22)	20.161(10)	2127(115)
B9-429	44.40(28)	20.125(10)	1935(112)
B9-432	41.95(24)	20.359(09)	1614(114)
B10-292	24.04(23)	21.622(19)	1145(105)
B10-583	25.08(30)	21.943(09)	2098(118)
B10-587	24.65(25)	21.745(15)	1695(108)
B10-590	24.41(25)	21.669(18)	1523(109)
B10-592	24.24(23)	21.653(21)	1337(107)
B10-617	36.26(28)	20.818(24)	2188(122)
B10-623	34.51(25)	20.947(19)	1784(112)
B10-627	34.51(30)	20.882(31)	1599(109)
B10-629	34.41(27)	20.847(33)	1445(107)
B10-632	34.28(30)	20.818(27)	1224(104)
B10-680	41.32(53)	20.480(17)	2152(140)
B10-685	41.05(34)	20.436(24)	1807(119)
B10-689	40.67(41)	20.383(18)	1540(107)
B10-694	42.23(31)	20.141(22)	1233(106)
B10-724	53.34(24)	19.823(09)	2446(119)
B10-725	53.15(45)	19.821(02)	2264(116)
B10-728	53.03(67)	19.767(57)	2033(113)
B10-732	52.76(40)	19.671(05)	1698(113)
B10-736	52.70(58)	19.622(11)	1440(110)
B16-363	39.65(33)	20.521(24)	2030(123)
B16-369	39.80(59)	20.468(44)	1760(110)
B16-376	39.85(72)	20.413(44)	1543(107)
B16-380	39.93(74)	20.341(12)	1341(105)
B16-388	39.49(22)	20.247(07)	1033(104)
B16-418	64.80(32)	19.043(09)	2207(118)

B16-430	64.96(35)	18.971(05)	1710(109)
B16-435	64.81(35)	18.936(05)	1439(106)
B16-443	64.80(33)	18.888(04)	1012(102)
B16-472	68.00(29)	18.859(13)	2073(113)
B16-485	67.99(29)	18.782(07)	1425(110)
B16-490	68.06(27)	18.758(08)	1249(104)
B16-530	78.75(40)	18.443(05)	2226(117)
B16-535	78.52(42)	18.390(04)	1689(110)
B16-539	78.48(29)	18.346(04)	1317(106)
B16-542	78.56(29)	18.321(04)	1099(104)
L17-481	3.10(12)	23.448(01)	300
L17-482	5.26(11)	23.155(03)	300
L17-483	7.98(10)	22.791(05)	300
L17-485	11.84(09)	22.307(05)	300
L17-486	14.59(08)	22.081(05)	300
L17-487	17.77(07)	21.747(12)	300
L17-489	20.73(07)	21.411(09)	300
L17-490	25.29(06)	21.064(12)	300
L17-491	30.61(06)	20.643(18)	300
L17-492	37.90(06)	20.193(14)	300
L17-493	39.93(10)	20.119(14)	300
L17-494	42.91(06)	19.973(31)	300

Fig. 1

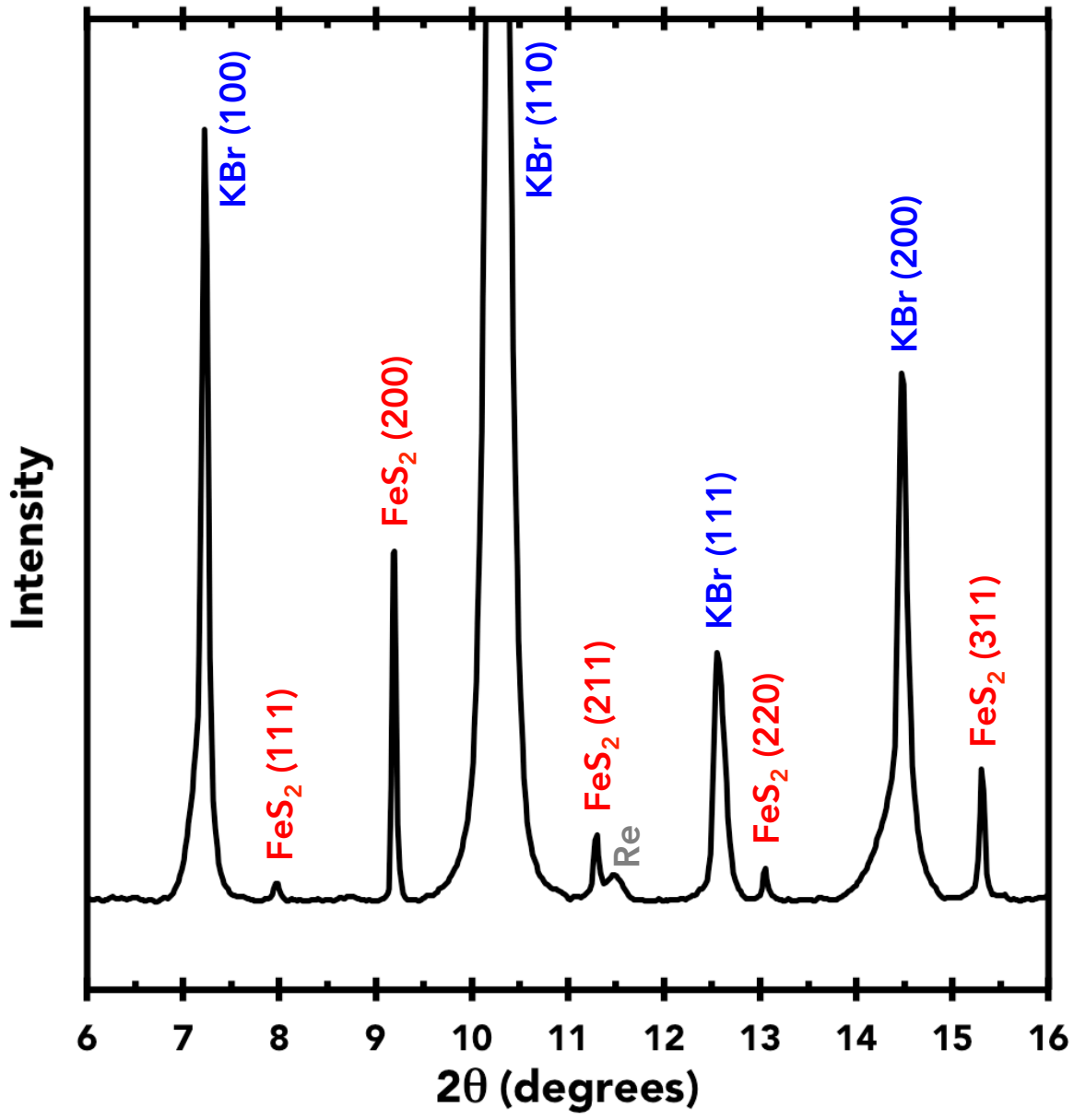
KBr (100)
FeS2 (111)
FeS2 (200)
KBr (110)
FeS2 (211)
Re
KBr (111)
FeS2 (220)
KBr (200)
FeS2 (311)
Intensity
6
7
8
9
10
11
12
13
14
15
16
2θ (degrees)

Fig. 2

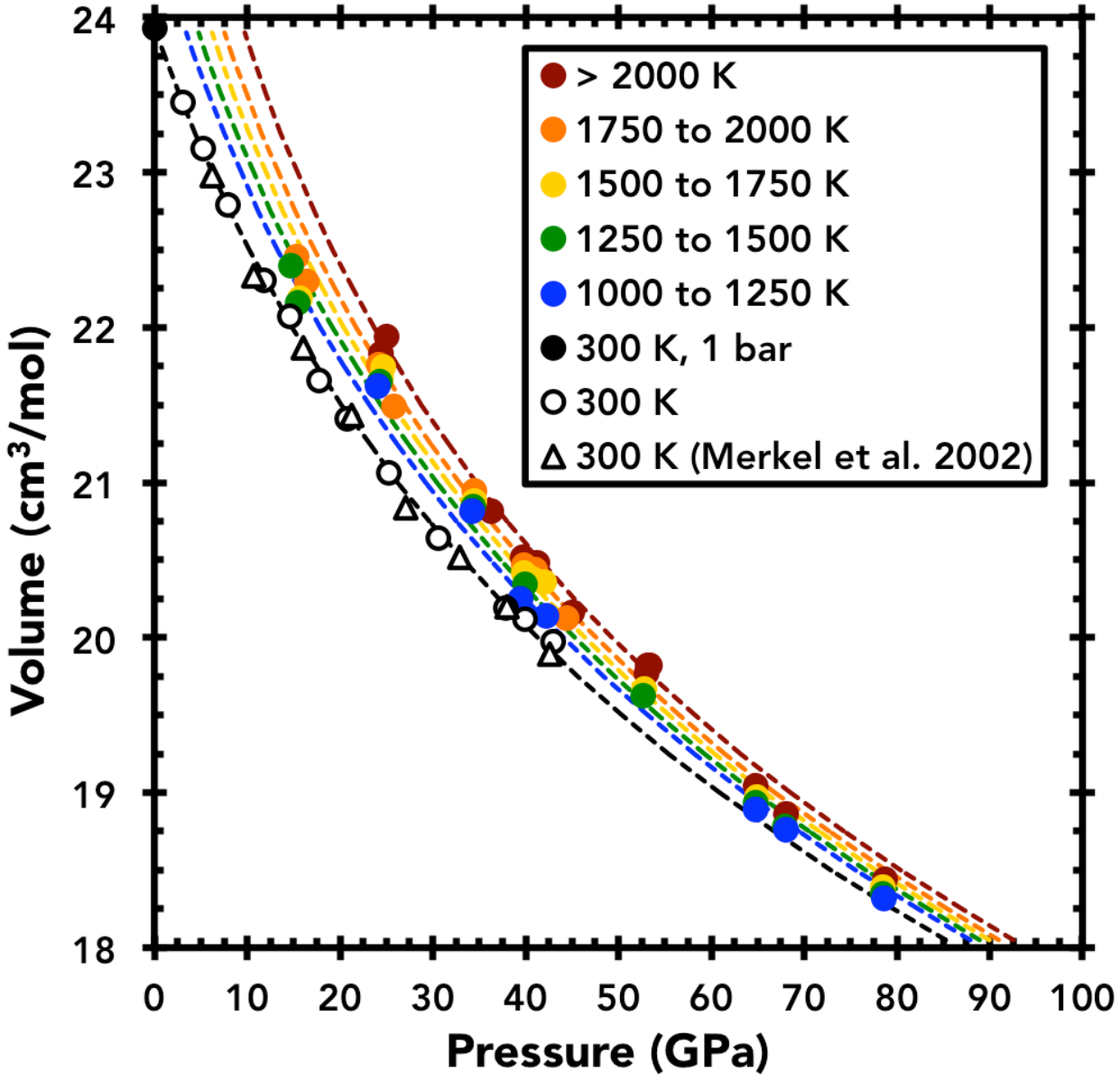
> 2000 K
1750 to 2000 K
1500 to 1750 K
1250 to 1500 K
1000 to 1250 K
300 K, 1 bar
300 K
300 K (Merkel et al. 2002)
Volume (cm³/mol)
Pressure (GPa)
24
23
22
21
20
19
18
0
10
20
30
40
50
60
70
80
90
100

Fig. 3

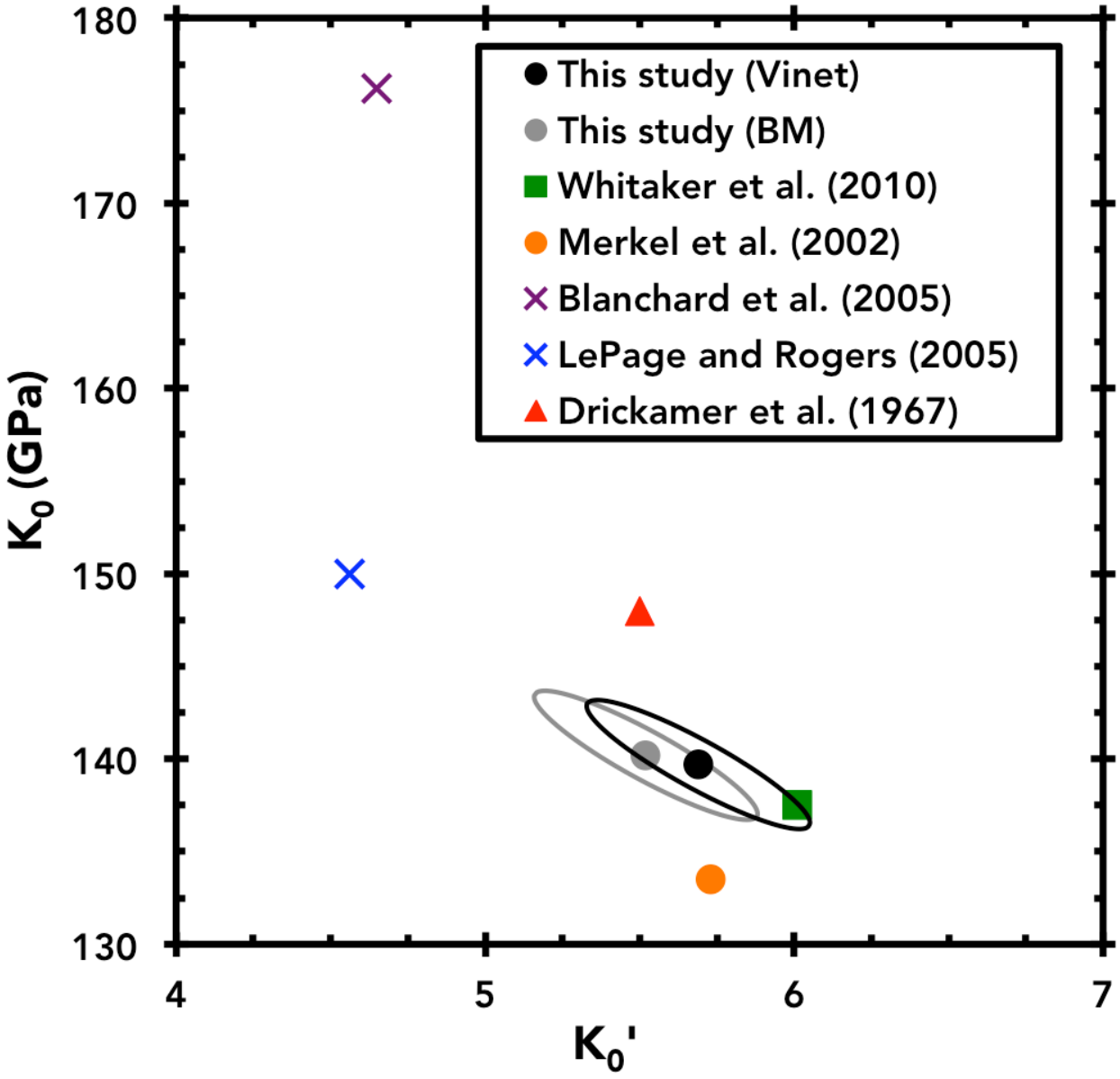
180
170
160
150
140
130
4
5
6
7
K_0 (GPa)
K_0'
This study (Vinet)
This study (BM)
Whitaker et al. (2010)
Merkel et al. (2002)
Blanchard et al. (2005)
LePage and Rogers (2005)
Drickamer et al. (1967)

Fig. 4a

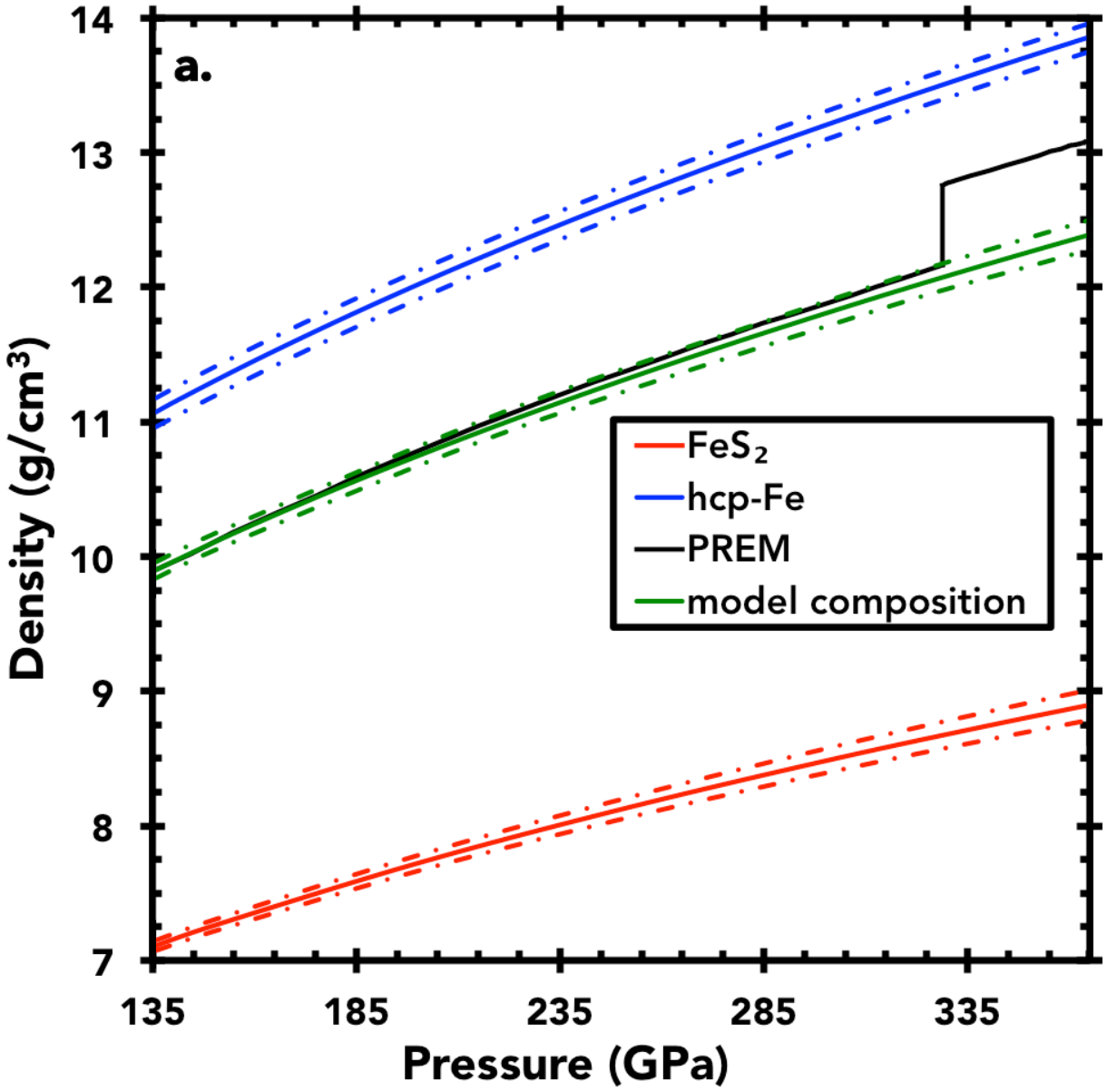
a.
14
13
12
11
10
9
8
7
Density (g/cm³)
135
185
235
285
335
Pressure (GPa)
FeS₂
hcp-Fe
PREM
model composition

Fig. 4b

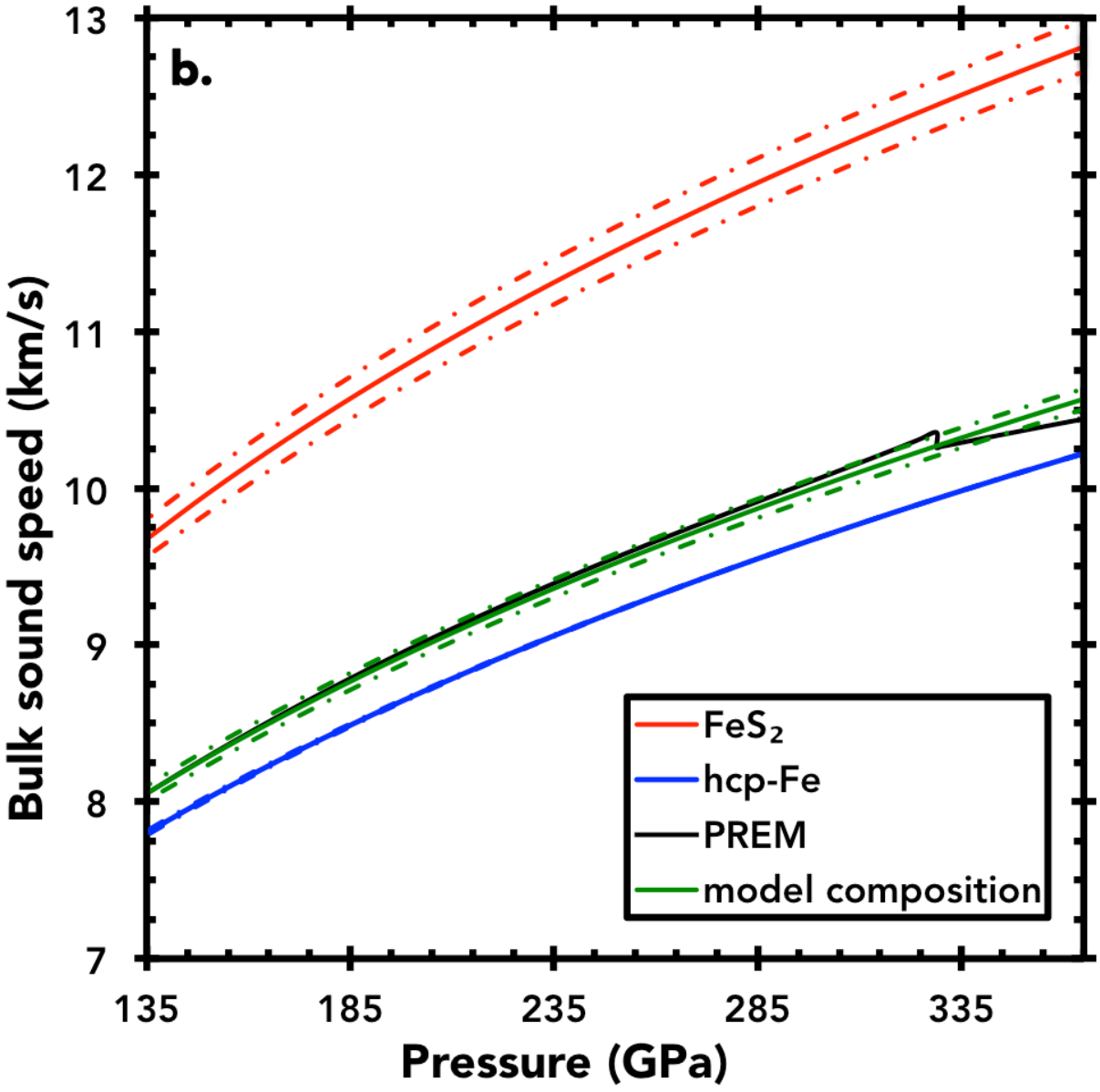
b.
Bulk sound speed (km/s)
Pressure (GPa)
13
12
11
10
9
8
7
135
185
235
285
335
FeS2
hcp-Fe
PREM
model composition

Fig. S1

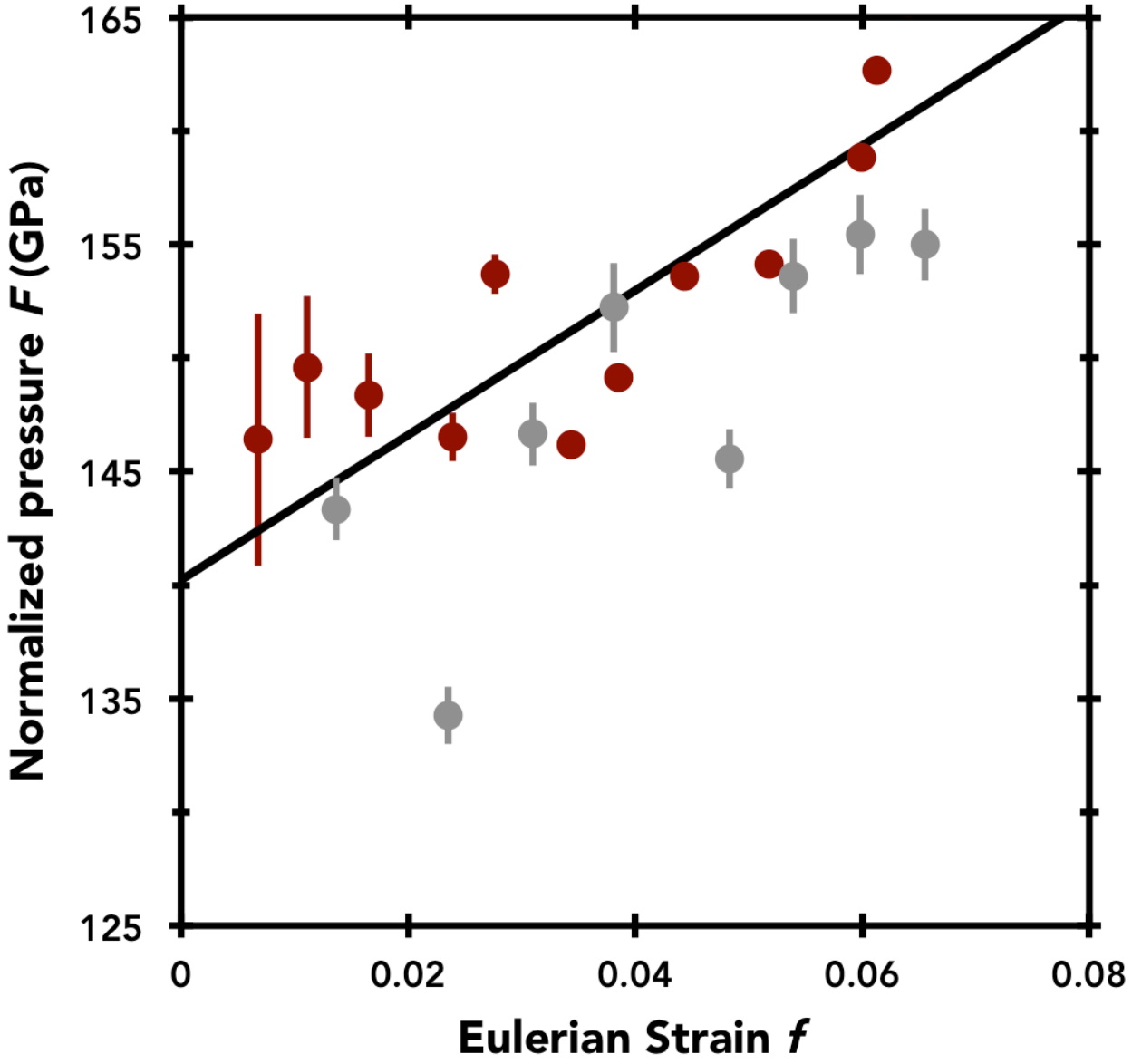
165
155
145
135
125
Normalized pressure F (GPa)
0
0.02
0.04
0.06
0.08
Eulerian Strain f

Fig. 2S

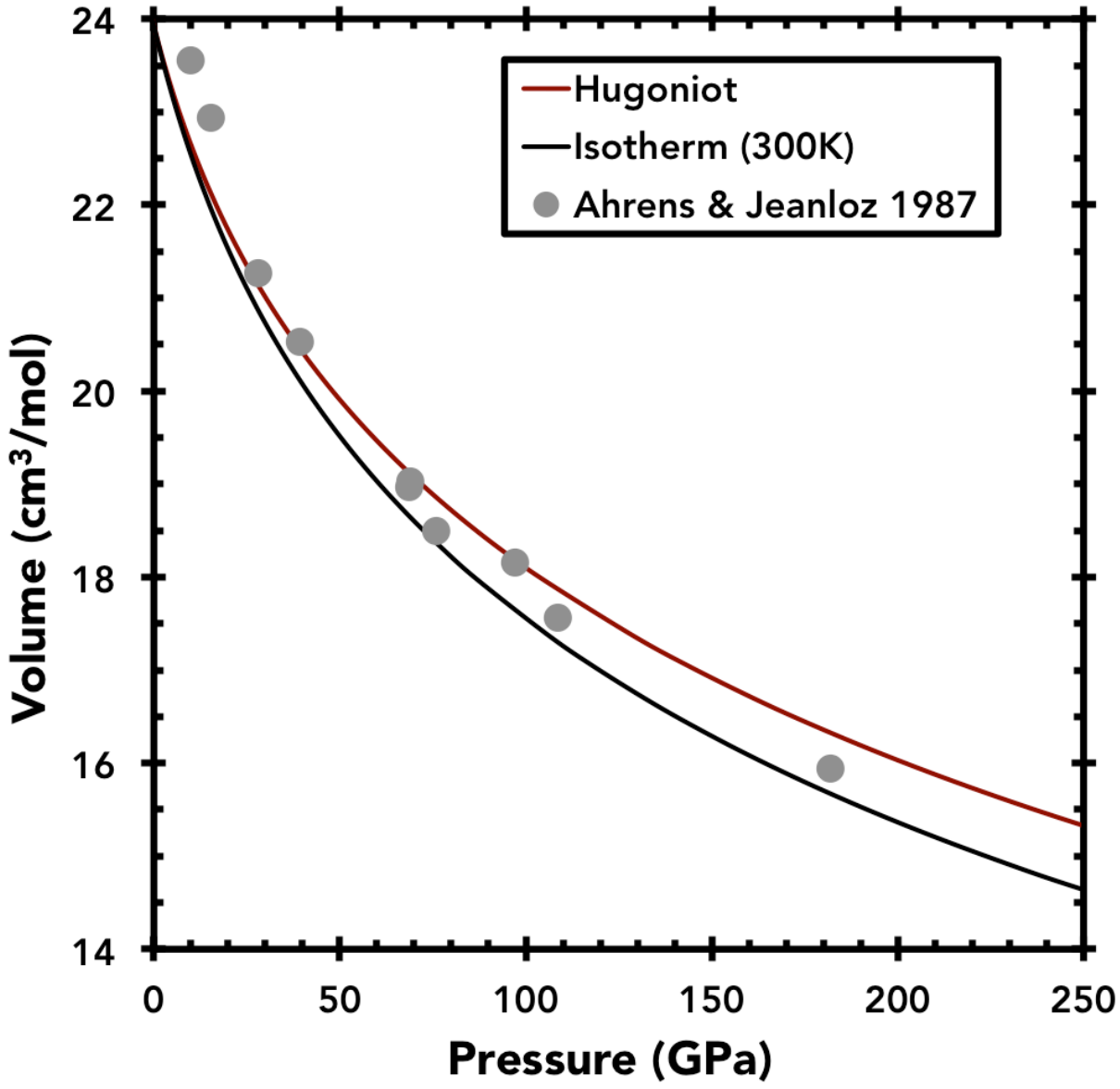
Hugoniot
Isotherm (300K)
Ahrens & Jeanloz 1987
Volume (cm³/mol)
Pressure (GPa)
24
22
20
18
16
14
0
50
100
150
200
250